



HAL
open science

Combining Rosetta's GIADA and MIDAS data: morphological versus dynamical properties of dust at 67P/Churyumov-Gerasimenko

A. Longobardo, T. Mannel, M. Kim, M. Fulle, A. Rotundi, V. Della Corte, G.
Rinaldi, J. Lasue, S. Merouane, H. Cottin, et al.

► To cite this version:

A. Longobardo, T. Mannel, M. Kim, M. Fulle, A. Rotundi, et al.. Combining Rosetta's GIADA and MIDAS data: morphological versus dynamical properties of dust at 67P/Churyumov-Gerasimenko. Monthly Notices of the Royal Astronomical Society, 2022, 516, pp.5611-5617. 10.1093/mnras/stac2544 . insu-03839367

HAL Id: insu-03839367

<https://insu.hal.science/insu-03839367>

Submitted on 7 Apr 2023

HAL is a multi-disciplinary open access archive for the deposit and dissemination of scientific research documents, whether they are published or not. The documents may come from teaching and research institutions in France or abroad, or from public or private research centers.

L'archive ouverte pluridisciplinaire **HAL**, est destinée au dépôt et à la diffusion de documents scientifiques de niveau recherche, publiés ou non, émanant des établissements d'enseignement et de recherche français ou étrangers, des laboratoires publics ou privés.

Combining Rosetta’s GIADA and MIDAS data: morphological versus dynamical properties of dust at 67P/Churyumov–Gerasimenko

A. Longobardo,¹★ T. Mannel,² M. Kim,² M. Fulle,³ A. Rotundi,⁴ V. Della Corte,¹ G. Rinaldi,¹ J. Lasue,⁵ S. Merouane,⁶ H. Cottin,⁷ M. Ciarniello,¹ F. Dirri¹ and E. Palomba¹

¹INAF-IAPS, via Fosso del Cavaliere 100, I-00133 Rome, Italy

²Space Research Institute of the Austrian Academy of Sciences, Schmiedlstrabe, 6, A-8042 Graz, Austria

³INAF-OATs, Via G.B. Tiepolo 11, I-34143 Trieste, Italy

⁴Università di Napoli ‘Parthenope’, DIST, Centro Direzionale Isola C4, I-80143 Naples, Italy

⁵IRAP-Roche, 44346, F-31028 Toulouse Cedex 4, France

⁶Max Planck Institute for Solar System Research, Justus-von-Liebig-Weg 3, D-37077 Göttingen, Germany

⁷Univ Paris Est Creteil and Université de Paris, CNRS, LISA, F-94010 Créteil, France

Accepted 2022 September 4. Received 2022 September 4; in original form 2022 May 26

ABSTRACT

We related morphological (size/shape) and dynamical properties of the dust ejected from the 67P/Churyumov–Gerasimenko comet by combining data from two instruments onboard the ESA’s Rosetta mission, i.e. the MIDAS atomic force microscope and the GIADA dust detector. The two instruments detected dust of different size (10^{-6} – 10^{-5} and 10^{-4} – 10^{-3} m, respectively). MIDAS detected dust in four periods, three during the inbound orbit arc (2014 September–November; 2014 December–2015 February; 2015 February–March) and one corresponding to a post-perihelion outburst (2016 February 19). For these periods, we analysed the dust particles’ spatial distribution on the MIDAS targets to obtain the number of parent particles hitting the instrument by means of an empirical procedure and to measure the corresponding dust flux. For the same periods, we retrieved the dust flux measured by GIADA. The ratio between the two dust fluxes is constant. By coupling this result with activity models, we inferred that the particles detected by MIDAS are fragments of hundreds-micron- to mm-sized particles detected by GIADA. In addition, the similar dust flux ratios between nominal activity and outburst indicates that the outburst did not include micro- and nano-sized dust, differently from other outbursts previously observed. Dust and surface properties were related by applying a traceback algorithm to GIADA data to retrieve the source regions of dust ejected in different periods. We did not detect variations of morphological properties between dust ejected from more and less processed terrains, concluding that compact dust particles (detected by MIDAS) have the same properties across the comet surface.

Key words: instrumentation: detectors – methods: data analysis – comets: general – comets: individual: 67p/Churyumov–Gerasimenko.

1 INTRODUCTION

The ESA/Rosetta mission escorted the 67P/Churyumov–Gerasimenko (hereafter referred to as 67P) comet from 2014 to 2016 and monitored its dust and gas activity along the orbital arc including perihelion, occurring on 2015 August 13. The Rosetta orbiter included several instruments and sensors to monitor the dust activity throughout the entire mission.

GIADA (Grain Impact Analyser and Dust Accumulator; Della Corte et al. 2014) detected dust particles belonging to two different porosity populations (Fulle et al. 2015; Rotundi et al. 2015): fluffy particles (porosity larger than 95 per cent) are the most pristine particles from the interstellar nebula (Fulle & Blum 2017) and range in size from 0.2 to 2.5 mm, while compact particles (i.e. porosity lower than 95 per cent) are more processed and range in

size from 0.03 to 1 mm. A traceback procedure has been developed by Longobardo et al. (2019) to associate each dust particle detected by GIADA with the corresponding surface source. The application of this procedure led to the conclusion that fluffy particles are more abundant in rough terrains (Longobardo et al. 2020), which are the least processed from cometary activity. This result has confirmed comet formation model predictions (Fulle et al. 2020), according to which fluffy particles were embedded within cm-sized pebbles (which are also responsible of roughness increase, as found, e.g. by Pajola et al. 2017). GIADA also detected nanogram dust, mainly during perihelion (Della Corte et al. 2019).

MIDAS (Micro-Imaging Dust Analysis System) collected μ m-sized particles and investigated their 3D structure (Bentley et al. 2016), finding that they are hierarchical dust agglomerates of smaller subunits, i.e. the smallest 67P units detected so far (Mannel et al. 2019). All particles detected by MIDAS are compact, except one extremely porous particle with a fractal structure similar to GIADA’s fluffy particles (Mannel et al. 2016). This is because the instrument

* E-mail: andrea.longobardo@inaf.it

Table 1. Exposure periods of MIDAS targets.

Target	Exposure period	67P orbit stage	#dust particles
10	2014 September–November	Inbound arc	383
12	2014 December–2015 February	Inbound arc	73
13	2016 February 19	Post-perihelion outburst	1607
14	2015 February–March	Inbound arc	10

was designed to detect the smallest particles, while fluffy particles are generally mm-sized.

The dust particles detected by COSIMA (Cometary Secondary Ion Mass Analyser) are tens of μm -sized solid and porous fragments (Merouane et al. 2017), both belonging to the compact dust population (Güttler et al. 2019). Most fragments are generated from the dust impact on the instrument funnel, but it was possible to retrieve the number of parent particle hitting COSIMA, due to the procedure by Merouane et al. (2017), based on comparison with simulations.

Rosetta results allowed Fulle et al. (2020) to develop of a new model of cometary activity, which concluded that activity is driven by the diffusion of gas sublimating from ices embedded in the dust particles composing the pebbles in the nucleus. The model also relates the dust size ejected by water-driven activity with the surface temperature, finding that no particles smaller than 1 mm could be ejected when surface temperature is 220 K (e.g. temperature reached in late 2014, Tosi et al. 2019), while particles of tens of microns could be ejected at perihelion.

In addition to this nominal activity, outburst events, i.e. sudden and short increase of dust ejection, have been observed during perihelion and post-perihelion stages (e.g. Bockelee-Morvan et al. 2017; Lin et al. 2017; Rinaldi et al. 2019). A few outbursts showed a dust colour change from red to blue, revealing the presence of very small particles (≤ 100 nm) (Bockelee-Morvan et al. 2017). On 2016 February 19, an outburst has been simultaneously observed by nine Rosetta instruments (Grün et al. 2016), with dust instruments detecting a signal enhancement (i.e. dust counts or dust brightness) of a factor larger than 10.

This work aims at deepening our knowledge of dust at 67P by combining the data from the GIADA and MIDAS dust detectors (with support of COSIMA data). The two instruments are complementary both in terms of dust size (μm -sized particles detected by MIDAS versus mm-sized particles detected by GIADA) and scientific information (physical properties measured by MIDAS versus dynamical properties measured by GIADA), therefore their data fusion allows us the characterization of dust activity in the periods where MIDAS detected dust, including the February 19 outburst. Moreover, the application of the traceback procedure by Longobardo et al. (2019) allows us to relate dust physical and surface geomorphological properties, enabling a small-scale study of the 67P's surface.

Data are presented in Section 2, while Section 3 summarizes previously developed procedures that are re-applied in this work. Data analysis is shown in Section 4, with results and related interpretation given in Sections 5 and 6, respectively. Finally, Section 7 is devoted to conclusions.

2 DATA

MIDAS was the Atomic Force Microscope (AFM) onboard the Rosetta spacecraft (Riedler et al. 2007); its operational modes are summarized by Bentley et al. (2016). It consists of several targets, each having a size of $2.4 \text{ mm} \times 1.4 \text{ mm}$ and exposed in a specific mission period.

For each target, the dust collection start time and end time are known. Therefore, for each particle detected by MIDAS, the available information is not the exact detection time but the detection period (lasting from days to weeks).

A single AFM scan swipes an $80 \mu\text{m} \times 80 \mu\text{m}$ area and lasts 6–12 h, therefore the detected particles are μm - to tens-of- μm -sized. After acquisition of a few scans, MIDAS continued to scan only in the case dust particles were detected. For this reason, target scanned areas are different.

Particles were detected by four targets, i.e. Target 10, Target 12, Target 13, and Target 14. Target 10 detected dust particles in three different ensembles of exposure periods (EEPs) between 2014 September and November, and hereafter referred to as 10A (scanned area of $2.29 \mu\text{m}^2$), 10B ($2.8 \mu\text{m}^2$), and 10C ($17.8 \mu\text{m}^2$). The four EEPs of Target 12 (hereafter 12A, 12B, 12C, and 12D, with corresponding scanned areas of 1.22, 2.35, 2.35, and $5.6 \mu\text{m}^2$, respectively) are included between 2014 December and 2015 February, while the three EEPs of Target 14 (hereafter 14A, 14B, and 14C, with corresponding scanned areas of 0.74, 0.73, and $0.97 \mu\text{m}^2$, respectively) correspond to the period 2015 February–March. Only Target 13 detected dust particles after perihelion; in particular, all the Target 13 particles are considered to be detected during the outburst occurring on 2016 February 19 in an exposed area in $42.94 \mu\text{m}^2$.

Table 1 shows exposure period of each target. Further details of the MIDAS data set are given by Kim et al. (in preparation).

GIADA included three subsystems. The Grain Detection System (GDS) was a laser curtain with photodiodes, which measured the particles' speed. Most of GDS detections were dust showers, i.e. ensembles of dust fragments created from the disruption of fluffy particles (Fulle et al. 2015). However, single (i.e. not grouped) GDS detections are commonly associated with compact particles (Longobardo et al. 2019). The Impact Sensor (IS) was a plate connected with piezoelectric sensors which measured particles' momentum and cross section. It detected only compact particles. The size range of particles detected by both GDS and IS spans from hundreds of microns to tens of mm (Fulle et al. 2015; Rotundi et al. 2015). The Quartz Crystal Microbalances measured cumulative mass of nanogram particles coming from different directions (Della Corte et al. 2019).

Because MIDAS detected only compact particles, we selected from GIADA data only the individual compact particles, i.e. the IS data set and single GDS detections (Longobardo et al. 2019; Rotundi et al. 2019).

The interpretation of our results was supported from analysis of COSIMA data. The COSIMA mass spectrometer includes 24 target holders, each having an area of $1 \text{ cm} \times 1 \text{ cm}$ (Kissel et al. 2007). For this work, we used three sets of targets which collected particles in periods overlapping the MIDAS exposition periods (i.e. 2014 August to December, 2014 December to 2015 February, 2015 February to April). The COSISCOPE camera imaged the targets on a regular basis (roughly once a week) during the exposure period, providing the number of particles detected by COSIMA. Particles detected by

COSIMA have a size of tens of microns and consist of fragments created from the impact of parent particles on the instrument funnel and/or target (Langevin et al. 2016; Merouane et al. 2017).

3 TOOLS

We took advantage of procedures developed in previous works to obtain additional information on GIADA and COSIMA data.

The traceback procedure developed by Longobardo et al. (2019, 2020) was applied to the IS data to associate each dust particle with the corresponding surface geomorphological region. The first step of the procedure was to retrieve the speed v of each particle by applying the empirical relation $v = Am^\gamma$ (Della Corte et al. 2016), where A and γ are parameters depending on the heliocentric distance and the phase angle, $m = p/v$ is the particle mass, and p is the momentum measured by IS. Then, we classified the geomorphological regions in two groups, based on description of the 67P regions given by El-Maarry et al. (2015, 2016), i.e. rough and smooth terrains. Details on the classifications are given by Longobardo et al. (2020). Finally, to associate dust particles and ejecting regions, we made the following assumptions: (a) radial motion in a non-rotating frame; (b) uniform acceleration up to a height of 11 km and constant speed above that height. On the basis on these assumptions, we obtained the time of flight of each dust particle, and, by taking into account the comet rotation, the terrain from which each dust particle comes. The accuracy of the assumptions, the extent of the procedure validity, and the role of geomorphological regions shape depend on the spacecraft altitude (Longobardo et al. 2020). The obtained results are generally reliable for altitudes lower than 70 km, even if uncertainty is larger above 50 km (Longobardo et al. 2020). Three MIDAS targets were exposed when the average spacecraft altitude was well below this limit (less than or about 30 km). Only Target 14 was exposed when the average spacecraft altitude was about 55 km, and in Section 6 we will discuss how this affected our results.

Another information retrieved from GIADA data is the dust density. This has been obtained from GDS+IS detections, by combining the cross section (measured by GDS) and the mass (obtained from the ratio of the momentum measured by IS and the speed measured by GDS) of each dust particle, and assuming a spheroidal shape (Fulle et al. 2016). We obtained a density average value for each of the periods corresponding to the exposition of a MIDAS target. Two different methods were used to retrieve these mean values: in the first one, the density of each dust particle was retrieved and then the mean density was obtained by averaging on all these density values; in the second one, we calculated the mean mass and the mean cross section, which were then considered to retrieve the mean density. The two methods provide quite different results, but, whatever the method, we obtain that the mean density is lower for two exposition periods and higher for the other two. Therefore, we identify two categories of density, indicated as ‘density $< 1000 \text{ kg m}^{-3}$ ’ (light particles) and ‘density $> 1000 \text{ kg m}^{-3}$ ’ (dense particles).

To compare the MIDAS and GIADA data with the COSIMA data, we considered that the particles detected by COSIMA are fragments of parent particles ejected from the comet surface and then disrupting when impacting on the COSIMA funnel. To retrieve the number of parent particles, we adopted the procedure by Merouane et al. (2017). The latter consists in comparing the dust distribution within a cluster with a random distribution developed by Monte Carlo simulations: particle clusters which can be modelled by a random spatial distribution with a probability lower than 5 per cent are assumed to be generated from the fragmentation of a single parent particle.

4 METHODS

4.1 MIDAS

Except for one case of fluffy agglomerate, all the dust particles detected by MIDAS are compact particles (Mannel et al. 2016). Particles detected by MIDAS are mostly fragments of parent particles ejected from the comet surface and then disrupted from the impact with the instrument funnel and/or targets. Because the compact particles detected by GIADA are parent particles, a reliable comparison between the two instruments is reliable only if we retrieve the number of parent particles which reached the MIDAS targets.

Two methods were developed for this aim. The mean shift algorithm, comparing the dust spatial distribution on the MIDAS targets with a theoretical one, is presented by Kim et al. (in preparation). Here, we show the empirical procedure. This method requires some assumptions, which will be discussed a posteriori in Section 6.2.

We assumed that dust particles clustered in the same target within two times the particle size and detected in the same exposition period belong to the same parent particles (Fig. 1).

The retrieved number of parent particles for each target (and corresponding exposition period) is summarized in Table 2.

Then, for each target we obtained a dust flux indicator (DFI, in the following text we will use the terms DFI and flux as synonyms). In order to obtain a reliable comparison between fluxes measured in different exposition periods, we should take into account the different target’s area scanned in different periods. Therefore, our DFI is obtained for each EEP by dividing the number of parent particles by the duration of the EEP, the square of the comet-spacecraft average distance, and the fraction of the target’s area scanned. The dust flux corresponding to each target is calculated as the average between the fluxes calculated in the EEPs of the target (the average was weighted over the duration of the EEPs). Because we are interested in studying the temporal flux variations, in the dust flux retrieval we did not consider parameters that are temporally constant and therefore do not affect the results of our study (e.g. the instrument cross section).

To study the physical properties of the dust particles coming from different regions, we analysed the dust shape distribution on the four targets. The parameter used as shape descriptor is the flatness (or aspect ratio), defined as $= h/\sqrt{A}$, where h and A are the particle height and area, respectively (Lasue et al. 2019; Kim et al., in preparation). A small F (i.e. close to zero) indicates a large/flattened particle, while a large one (i.e. close to 1) indicates a spherical particle. We discarded particles imaged at poor-resolution, not sufficient to give a reliable F value (Kim et al., in preparation).

4.2 GIADA

The individual compact particles detected by the GIADA-IS are not fragmented, so we do not need a procedure as that applied on MIDAS data. We retrieved the dust flux measured by GIADA for each of the four MIDAS exposition periods. For simplicity, hereafter we will label the four period with same name of the corresponding MIDAS targets, i.e. 10, 12, 13, and 14. The dust flux was calculated by dividing the number of detected particles by duration of the period and the square of the average comet-spacecraft distance. Also in this case, the flux corresponding to each period was calculated as weighted average between the different EEPs included in each period, considering the EEP’s duration as weight. As for MIDAS, the flux is calculated excluding constant parameters which do not affect the study of its temporal variation.

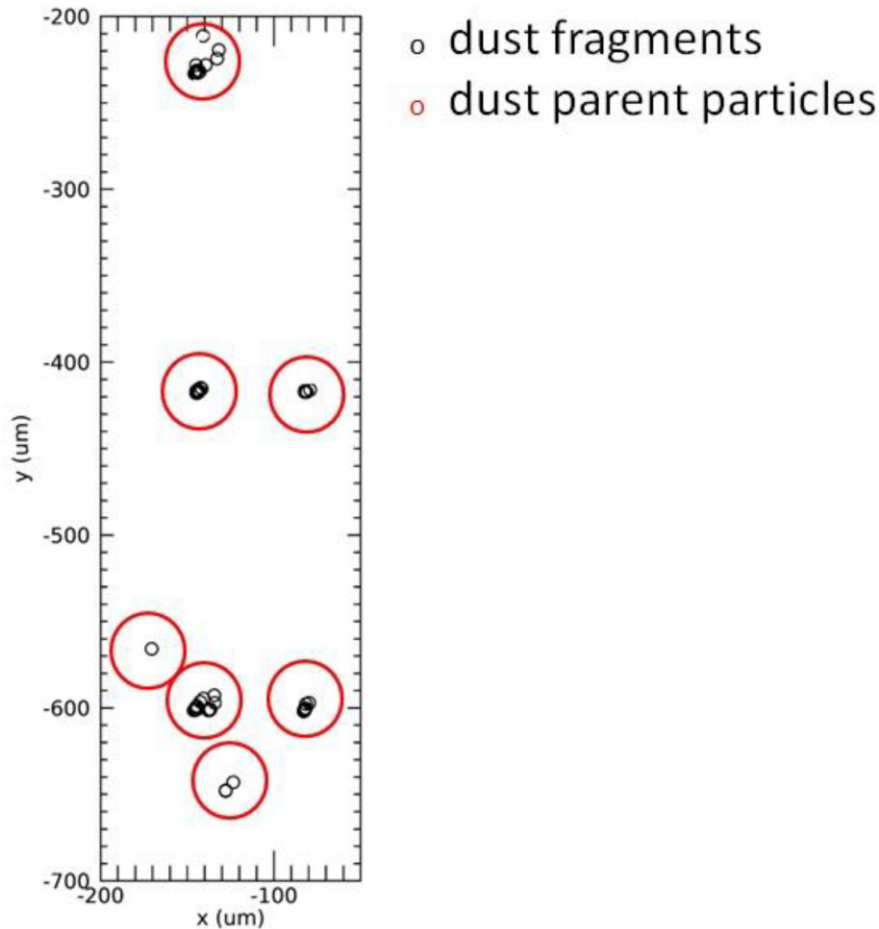


Figure 1. Example of retrieval of parent particles hitting the MIDAS target. The example in the figure refers to a scanned portion of the Target 13. Each black circle corresponds to the location of a particle detected by MIDAS. The red circles enclose particles belonging to the same parent particle. Each red circle includes particles whose relative distance is lower than two times the particle size. The particle size is not reported for clarity. Note that the size of red circles does not correspond to the size of parent particles.

Table 2. Retrieved number of dust compact parent particles hitting the MIDAS targets.

Target	Parent particles
10	69
12	29
13	377
14	3

Moreover, for each period, we calculated the average dust particle speed and density retrieved by the GIADA IS and GDS+IS, respectively.

Finally, for each of the four periods under study, we identified the surface regions which ejected the dust particles detected by GIADA by applying the traceback algorithm and calculated the percentage of dust particles coming from smooth and rough terrains, respectively.

4.3 Data fusion

We calculated the ratio between the dust fluxes measured by MIDAS and GIADA, respectively, in the four periods when MIDAS detected particles. The retrieved ratio does not include constant parameters

(e.g. the instrument cross sections) which do not affect the study of the flux ratio temporal behaviour.

The data fusion between MIDAS and GIADA also allowed us to study the physical properties of dust particles ejected from terrains with different geomorphology (i.e. rough and smooth). The application of the traceback procedure on the GIADA IS data allowed us to infer the source regions of the particles collected on the MIDAS targets. Then, the study of the flatness distribution of the particles collected on the four targets gave us the possibility to characterize the different geomorphologies at the dust scale.

5 RESULTS

The largest DFIs are measured during the outburst, i.e. in the Period 13. For both instruments, the DFI obtained for Period 10 is one order of magnitude lower, while those obtained for Periods 12 and 14 are two orders of magnitude lower.

Table 3 shows the DFI ratio between MIDAS and GIADA in the four periods studied. This ratio is constant within the uncertainties.

The average dust speed and density calculated from GIADA for the four exposition periods are summarized in Table 4. During periods 13 and 14 faster and lighter dust particles were detected.

From the traceback procedure (Longobardo et al. 2020), we retrieved that almost all particles detected on the Target 13 come

Table 3. Ratio between the dust flux indicator calculated from MIDAS and GIADA data for the periods corresponding to the MIDAS targets' exposition periods.

Period	MIDAS/GIADA DFI
10	4.6 ± 0.8
12	6.1 ± 1.5
13	4.6 ± 0.4
14	3 ± 2

Table 4. Mean speed and density of the dust particles detected by GIADA in the four MIDAS' EEPs.

Period	Mean dust speed (m s^{-1})	Dust density (g cm^{-3})
10	3.2 ± 1.5	>1000
12	2.7 ± 0.3	>1000
13	7.21 ± 0.09	<1000
14	6.8 ± 0.5	<1000

from pristine terrains, i.e. rough terrains (Anhur, Bes, and Khephry), which are the less processed 67P's terrains, and deeper comet layers, as expected in outbursts (Agarwal et al. 2017). More than 60 per cent of particles detected by GIADA in Period 14 are ejected from the Hapi region, which is a smooth terrain. Finally, the regions ejecting dust particles in Periods 10 and 12 are almost equally divided in rough (Ash and Seth) and smooth (Hapi and Ma'at) terrains.

Despite the different source region, the flatness distribution of the dust particles on the different MIDAS targets is very similar, as shown in Fig. 2.

6 DISCUSSION

6.1 Dust flux in different periods

The largest flux is measured during the outburst, while the nominal activity DFI (Period 10) is one order of magnitude lower. Fluxes measured during Periods 12 and 14 are two orders of magnitude lower than the outburst. We ascribe this difference among nominal activity fluxes to unfavourable observations conditions during periods 12 and 14. In particular, the particles detected during Period 12 are the slowest one (Table 4) and therefore more likely to be deviated from their radial path (particles detected during Period 10 have a similar average speed, but a large speed spread, hence it is likely that the flux is more affected by faster particles). Dust particles detected during Period 14 are also likely to be deviated, due to the largest spacecraft altitude (see Section 3).

6.2 Dust flux ratio during nominal activity and outburst

Table 3 shows that the ratio between dust fluxes measured by MIDAS and GIADA is constant within errors, i.e. the ratio between μm - and mm -sized particles is constant. However, according to activity models (Fulle et al. 2020), the surface temperature reached in these periods does not allow ejection of μm -sized particles by nominal activity. Combining this information, we conclude that MIDAS and GIADA detect dust particles of the same size: in particular, the μm -sized particles detected by MIDAS are fragments of larger dust particles, as those detected by GIADA.

However, this result could be affected by our initial assumption that each parent particle hitting MIDAS generates a single dust cluster (i.e. the ensemble of particles within two times the particle size)

on the target after its fragmentation. Nevertheless, this assumption agrees with the experiments by Ellerbroek et al. (2017), which shot low-velocity (i.e. a few m s^{-1} , similar to those measured by GIADA) dust particles having size up to $400 \mu\text{m}$ (similar to the dust particle size detected by GIADA in these periods, see the next subsection).

We calculated the DFI ratio by considering the number of parent particles obtained from the mean shift algorithm (Min et al., in preparation), too: also in this case, we found that it is constant within uncertainties.

Finally, we compared the obtained flux ratios with those obtained considering the dust flux ratio between COSIMA and GIADA. COSIMA detected dust in a size range overlapping with MIDAS and the corresponding fluxes were calculated by considering the parent particles hitting the instrument. The comparison was done only for Periods 10 and 12, because during Period 13 the COSIMA shutter was closed, while for Period 14 the ratio has an uncertainty larger than 100 per cent and therefore it is a meaningless result. Table 5 shows that the COSIMA-to-GIADA DFI ratio is constant as in the case of the MIDAS-to-GIADA DFI ratio. This gives further evidence that micron to tens to microns particles are fragments of larger particles.

A more detailed analysis was done for Period 13, because outburst activity did not follow the nominal activity model and ejection of small particles (i.e. up to 0.1-micron size) during an outburst has been observed by Bockelee-Morvan et al. (2017). In principle, we could expect a larger MIDAS/GIADA DFI ratio for Period 13, because MIDAS would collect not only fragments of mm -sized particles (detected by GIADA), but also micron-sized particles directly ejected from the comet surface (not detected by GIADA). This DFI ratio increase is not observed. Otherwise, the DFI ratio even decreases (even if within uncertainty) if we consider the number of parent particles retrieved by Min et al. (in preparation). This means that during the 2016 February 19 outburst no micron- and nm -sized particles were ejected, differently than the 2015 August outburst (Bockelee-Morvan et al. 2017). This result agrees with observations of other instruments of the same outburst, i.e.:

- (i) Rosetta's remote observations (from OSIRIS, ALICE, and Star Tracker instruments) did not show occurrence of such particles (Grun et al. 2016);
- (ii) The GIADA's MicroBalance System (which detects only the lightest particles) did not record a mass increase during that outburst (Della Corte et al. 2019).

Finally, we performed a more detailed analysis on Period 12 because of its larger DFI ratio. Provided that this increase is within uncertainties and hence could just be due to statistics, we looked for possible contribution of other effects. We calculated the fragmentation ratio, i.e. the average number of fragments for each dust parent particle, from MIDAS data and the average dust speed from GIADA data for Periods 12 and 13, obtaining the values listed in Table 6.

Period 12's dust particles are slower, therefore less likely to be fragmented, as also evidenced by the lower fragmentation ratio (even if it is similar within errors) and consequently less likely to lose mass. This might explain the larger MIDAS/GIADA DFI ratio for Period 12, even if this is not significant. A similar relation between fragmentation ratio and particle speed has been observed by Kim et al. (in preparation).

6.3 Dust source

While in principle we could find variations of physical properties between compact dust coming from rough and smooth terrains, the

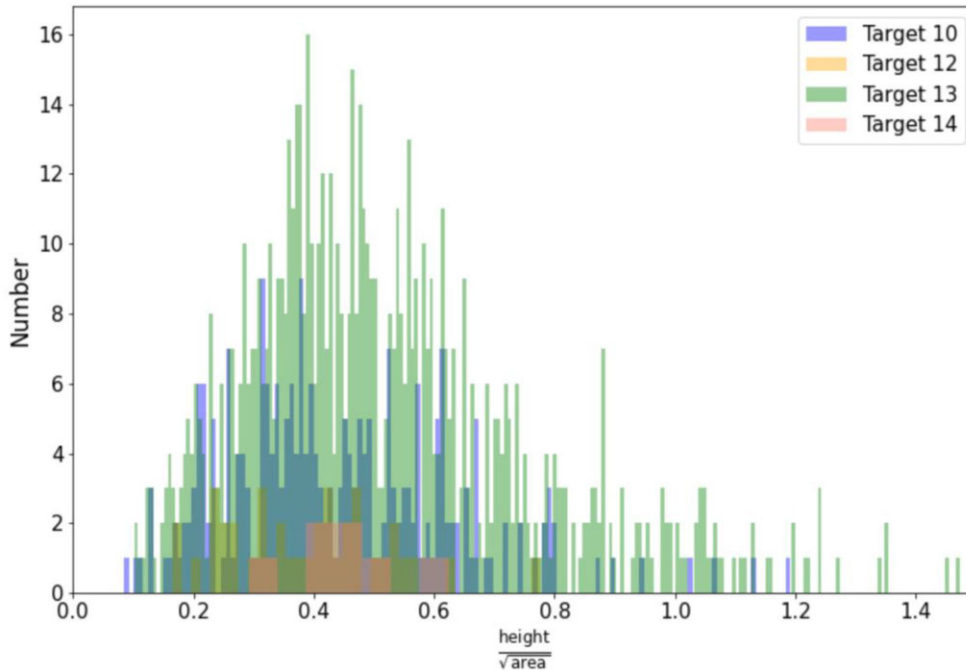


Figure 2. Histogram of the F parameter for the four different MIDAS targets.

Table 5. Ratio between the dust flux indicator calculated from MIDAS and GIADA data (second column) and from COSIMA and GIADA (third column) for the Periods 10 and 12.

Period	MIDAS/GIADA DFI	COSIMA/GIADA DFI
10	4.6 ± 0.8	2.2 ± 0.3
12	6.1 ± 1.5	2.8 ± 0.6

Table 6. DFI ratio, dust fragmentation ratio (i.e. average number of fragments for each parent particle hitting MIDAS), and dust average speed (measured by GIADA data) retrieved for Periods 12 and 13.

Period	MIDAS/GIADA DFI	Fragmentation ratio	Average speed (m s^{-1})
12	6.1 ± 1.5	2.5 ± 1.6	2.7 ± 0.03
13	4.6 ± 0.4	4 ± 2	7.21 ± 0.09

dust flatness distributions of the four targets are very similar. We also calculated the average dust particle size in the four periods, by considering the cross sections measured by GIADA (Fulle et al. 2016), obtaining a value of 400–500 μm for all periods. Other dust shape descriptors (elongation, circularity, convexity, surface/volume), calculated by Kim et al. (in preparation) for each target, have been found to be constant, too.

The only difference concerns density (Table 4). However, this is not related to the dust source because dust density is the same for Periods 13 and 14, corresponding to different roughness of ejecting regions. Rather, it is related to dynamical properties: when particles are faster (i.e. Periods 13 and 14), even the lighter ones reach the GIADA detectors (because they are less likely to be deviated) and therefore the average dust density is lower, and vice versa.

In conclusion, while the relative abundance of fluffy and compact particles changes from rough and smooth terrains (Longobardo et al.

2020), there is no link between compact particles shape and terrains roughness and/or evolution.

7 CONCLUSIONS

This work compared the dust fluxes measured by the GIADA and MIDAS instruments onboard Rosetta, after the application of an empirical procedure to retrieve the number of parent particles which hit the MIDAS targets and hence the average number of fragments generated by dust impacts on MIDAS.

In principle the two instruments provide complementary information about the dust size, because MIDAS and GIADA detected dust of size of a few microns and hundreds of microns, respectively. The constant flux ratio between the two instruments, confirmed by the comparison with fluxes measured by COSIMA and coupled with conclusions given by activity models (Fulle et al. 2020), led to the conclusions that particles detected by MIDAS are fragments of larger particles, these being detected by GIADA.

Assuming that particles detected in the same period by the two instruments come from the same regions, we applied the traceback algorithm by Longobardo et al. (2020) to the GIADA-IS data to study morphological properties (measured by MIDAS) of dust coming from smooth and rough terrains, respectively. No flatness/size variations are observed; therefore, these properties of compact dust particles are homogeneous across the 67P surface. The observed dust density variations are not related to source regions, but to their dynamics: when ejection speeds are larger, even lighter dust particles reach the detectors. These particles are more likely to be fragmented when impacting the MIDAS funnel and target.

During the 2016 February 19 outburst, the flux ratio between the two instruments does not change. This suggests that no micro- and nano-meter-sized dust was ejected during this outburst, according to measurements of other Rosetta instruments (microbalances, spectrometers). This is a different result with respect to the 2015 September outburst (Bockelee-Morvan et al. 2017).

ACKNOWLEDGEMENTS

To memory of our colleague Maria Teresa Capria.

This research was supported by the Italian Space Agency (ASI) within the ASI-INAF agreement I/032/05/0 and by the International Space Science Institute (ISSI) through the ISSI International Team ‘Characterization of cometary activity of 67P/Churyumov–Gerasimenko comet’.

GIADA was built by a consortium led by the Università degli Studi di Napoli ‘Parthenope’ and INAF – Osservatorio Astronomico di Capodimonte, in collaboration with the Istituto de Astrofisica de Andalucia, Selex-ES, FI, and SENER. GIADA is presently managed and operated by Istituto di Astrofisica e Planetologia Spaziali-INAF, Italy. GIADA was funded and managed by the Agenzia Spaziale Italiana, with the support of the Spanish Ministry of Education and Science Ministerio de Educacion y Ciencias (MEC). GIADA was developed from a Principal Investigator proposal from the University of Kent; science and technology contributions were provided by CISAS, Italy; Laboratoire d’Astrophysique Spatiale, France; and institutions from the UK, Italy, France, Germany, and the USA. Science support was provided by NASA through the U.S. Rosetta Project managed by the Jet Propulsion Laboratory/California Institute of Technology. We would like to thank A. Coradini for her contribution as a GIADA Co-Investigator. GIADA calibrated data are available through ESA’s Planetary Science Archive (PSA) website (<http://www.rssd.esa.int/index.php?project = PSA&page = index>).

MK and TM acknowledge funding by ESA project ‘Primitiveness of cometary dust collected by MIDAS onboard Rosetta’ (Contract No. 4000129476).

DATA AVAILABILITY STATEMENT

GIADA calibrated data are available through ESA’s Planetary Science Archive (PSA) website (<http://www.rssd.esa.int/index.php?project = PSA&page = index>).

REFERENCES

- Agarwal J. et al., 2017, *MNRAS*, 469, S606
 Bentley M.S. et al., 2016, *Nature*, 537, 73
 Bockelée-Morvan D. et al., 2017, *MNRAS*, 469, S443
 Della Corte V. et al., 2014, *J. Astron. Instrum.*, 3, 1350011
 Della Corte V. et al., 2016, *MNRAS*, 462, S210
 Della Corte V. et al., 2019, *A&A*, 630, A25
 El-Maarry M.R. et al., 2015, *A&A*, 583, A26
 El-Maarry M.R. et al., 2016, *A&A*, 593, A110
 Ellerbroek L.E. et al., 2017, *MNRAS*, 469, S204
 Fulle M. et al., 2015, *ApJS*, 802, L12
 Fulle M. et al., 2016, *ApJ*, 821, 19
 Fulle M. et al., 2020, *MNRAS*, 493, 4039
 Fulle M., Blum J., 2017, *MNRAS*, 492, S39
 Grün E. et al., 2016, *MNRAS*, 462, S220
 Güttler C. et al., 2019, *A&A*, 630, A24
 Kissel J. et al., 2007, *Space Sci. Rev.*, 128, 823
 Langevin. Y. et al., 2016, *Icarus*, 271, 76
 Lasue J. et al., 2019, *A&A*, 630, A28
 Lin Z.-Y. et al., 2017, *MNRAS*, 469, S731
 Longobardo A. et al., 2019, *MNRAS*, 483, 2165
 Longobardo A. et al., 2020, *MNRAS*, 496, 125
 Mannel T. et al., 2016, *MNRAS*, 462, S304
 Mannel T. et al., 2019, *A&A*, 630, A26
 Merouane S. et al., 2017, *MNRAS*, 469, S459
 Pajola M. et al., 2017, *MNRAS*, 469, S636
 Riedler W. et al., 2007, *Space Science Reviews*, 128, 869
 Rinaldi G. et al., 2019, *A&A*, 630, A21
 Rotundi A. et al., 2015, *Science*, 347, 6220
 Rotundi A., the International GIADA Consortium, 2019, Rosetta-Orbiter67P
 GIADA 5 Dust Maps V1.0, RO-C-GIA-5-67P-DUST-MAPS-V1.0.ESA
 Planetary Science Archive and NASA Planetary Data Systemext
 Tosi F. et al., 2019, *Nat. Astron.*, 31, 649

This paper has been typeset from a Microsoft Word file prepared by the author.